Int. J. Sci. R. Tech., 2026 3(4)
A Multidisciplinary peer-reviewed Journal
www.ijsrtjournal.com [ISSN: 2394-7063]

Original Article

Plant-Mediated Green Synthesis, Characterization and Applications of ZnO, BiO Nanoparticles and Their Zn-BiO Nanocomposite

J AshaJyothi*, Carolin Jeniba Rachel, Savari Susila

PG Department of Chemistry, St. Mary's College (Autonomous) Thoothukudi - 628001.

ABSTRACT

This study reports an eco-friendly green synthesis of zinc oxide (ZnO), bismuth oxide (BiO), and Zn–BiO nanocomposite using *Hydrocotyle verticillata* leaf extract as a natural reducing and stabilizing agent. This plant-mediated approach eliminates toxic chemicals and offers a simple, cost-effective, and sustainable route for synthesizing multifunctional nanomaterials. The nanoparticles were characterized using UV–Visible spectroscopy, FT-IR, XRD, FESEM, EDX, and TGA to evaluate their structural, optical, morphological, and thermal properties. UV–Visible analysis showed strong UV absorption for ZnO and enhanced visible absorption for BiO, while the Zn–BiO nanocomposite exhibited a red shift, indicating modified optical behavior. FT-IR confirmed Zn–O and Bi–O bond formation, and XRD revealed well-defined crystalline structures with nanoscale crystallite sizes. TGA demonstrated good thermal stability, with the nanocomposite showing improved stability due to strong interfacial interactions. FESEM images indicated distinct morphologies and better dispersion in the composite, while EDX confirmed elemental composition and high purity. Antibacterial studies showed moderate activity of ZnO against *Escherichia coli* and stronger activity of BiO against *Bacillus subtilis*. Corrosion studies revealed ZnO performs better in alkaline medium, BiO in neutral medium, and Zn–BiO shows superior inhibition in acidic conditions. Shelf-life studies demonstrated delayed vegetable spoilage, indicating effective antimicrobial performance. Overall, the Zn–BiO nanocomposite exhibits enhanced physicochemical properties and promising applications in antimicrobial, anticorrosion, and food preservation fields.

Keywords: Green synthesis, ZnO–BiO nanocomposite, Antibacterial activity, Corrosion inhibition, *Hydrocotyle verticillata* extract

INTRODUCTION

Zinc oxide nanoparticles (ZnO NPs) are nanosized materials (1–100 nm) with unique physical, chemical, and biological properties due to high surface area and quantum effects. They can be synthesized by physical, chemical, and green methods, with green synthesis—using plant extracts like *Hydrocotyle verticillata*—being eco-friendly, cost-effective, and producing stable, biocompatible nanoparticles. ZnO NPs exhibit semiconducting, photocatalytic, antimicrobial, UV-blocking, and antioxidant properties, enabling applications in medicine, environmental remediation, cosmetics, textiles, electronics, and agriculture. Their properties can be tuned by controlling size, shape, and surface characteristics. Bulk ZnO is a white, odorless, amphoteric compound with high thermal stability, crystallizing in a hexagonal wurtzite structure. It is a wide band-gap semiconductor (~3.3 eV) with strong UV absorption and n-type conductivity due to intrinsic defects. Additionally, it shows piezoelectric behavior, moderate mechanical strength, and notable biological activities such as antibacterial and biocompatibility, making it highly valuable across scientific and industrial fields. Zinc oxide (ZnO) nanoparticles are widely used due to their unique properties. In medicine, they exhibit strong antibacterial and antifungal activity by producing reactive oxygen species (ROS) and releasing zinc ions that damage microbes. Their biocompatibility also makes them suitable for drug delivery and cancer therapy, enabling targeted and controlled treatment [6-7].

Bismuth oxide (BiO) is a p-type semiconductor known for its polymorphic structures, narrow band

Relevant conflicts of interest/financial disclosures: The authors declare that the research was conducted in the absence of any commercial or financial relationships that could be construed as a potential conflict of interest.

gap, and strong visible-light photocatalytic activity. It exists in multiple phases (α, β, γ, δ, and ω), with α-Bi_2O_3 being the most stable at room temperature.[13] The polymorphic nature of BiO significantly affects its optical, electrical, and catalytic properties. With a narrow band gap (~2.0–2.8 eV), it efficiently absorbs visible light, making it well-suited for photocatalytic and environmental applications. Bismuth-based nanomaterials are relatively eco-friendly due to their low toxicity and good chemical stability. Recent studies emphasize doping to improve charge separation and hydrogen evolution, thereby enhancing photocatalytic efficiency by minimizing electron–hole recombination [12]. BiO nanoparticles show polymorphism with different crystal structures. The α-phase, which has a monoclinic structure, is stable at room temperature. Their crystal structure is analyzed using X-ray diffraction (XRD), while crystallite size and microstrain are determined using the Williamson–Hall method [16]. BiO is a p-type semiconductor with high oxygen ion conductivity, especially in the δ-phase at elevated temperatures. It is thermally stable, though phase transitions at higher temperatures can affect its photocatalytic performance [22]. BiO nanoparticles are effective for photocatalytic degradation of organic pollutants due to their narrow band gap and visible-light activity [15].

Zn–BiO nanocomposites integrate n-type ZnO with p-type BiO to form a p–n heterojunction, improving charge separation efficiency. Although ZnO has a wide band gap (~3.37 eV) and high exciton binding energy, its photocatalytic performance is limited by fast electron–hole recombination [14]. Coupling ZnO with BiO forms a heterojunction that enhances visible-light absorption and reduces electron–hole recombination, leading to improved photocatalytic and antimicrobial performance. Efficient charge separation at the interface increases catalytic activity. Additionally, Ag-doped ZnO–$NaBiO_3$ composites show superior visible-light photocatalysis, while doped $NaBiO_3$/ZnO systems exhibit enhanced antimicrobial effects due to increased ROS generation and better interaction with microbial cells [24]. ZnO–BiO heterojunction formation is confirmed by XRD analysis. Compared to pure materials, the composite typically shows smaller crystallite size and better lattice interaction. Crystallite size and strain can be evaluated using the Williamson–Hall method. These nanocomposites exhibit enhanced visible-light absorption, a reduced band gap, and longer charge carrier lifetime. The internal electric field at the p–n junction suppresses electron–hole recombination, leading to improved photocatalytic efficiency [23]. ZnO–BiO heterojunctions show improved degradation of dyes and organic pollutants under visible light due to efficient charge separation and reduced electron–hole recombination. They also exhibit strong antimicrobial activity through ROS generation, which damages microbial cells. Additionally, modified Zn–BiO systems enhance photocatalytic hydrogen production by promoting better electron utilization in hydrogen evolution [12].

MATERIALS & METHODS

a. Collection of plants

Fresh leaves of *Hydrocotyle verticillata* were collected from naturally growing plants in the local area. The collected leaves were washed thoroughly with running tap water to remove dust and adhering impurities, followed by rinsing with double distilled water. The cleaned leaves were shade-dried at room temperature for 7–10 days to prevent the degradation of heat-sensitive bioactive compounds. The dried leaves were stored in clean, airtight containers and used for the preparation of leaf extract.

b. Preparation of Leaf Extract

The shade-dried leaves of *Hydrocotyle verticillata* were finely powdered using a blender and stored in airtight containers at room temperature. Few grams of the powdered leaf material were transferred into a clean beaker containing 100 mL of distilled water. The mixture was heated at 60–80 °C for 20–30 minutes with continuous stirring to ensure efficient extraction of bioactive compounds. After heating, the extract was allowed to cool to room temperature and filtered through Whatman No. 1 filter paper. The clear filtrate obtained represented the aqueous leaf extract and was stored at 4 °C for further nanoparticle synthesis.

c. Synthesis of ZnO nanoparticles

For the synthesis of zinc oxide nanoparticles, few grams of zinc sulphate were added to the leaf extract of *Hydrocotyle verticillata* under continuous

sonication. The reaction mixture was maintained at 35 °C for 4 h. A visible color changes from green to brown along with turbidity indicate the reduction of zinc ions and the formation of ZnO precursor complexes mediated by the phytochemicals present in the leaf extract. The obtained filtrate was dried in a hot air oven until complete evaporation of moisture. The dried residue was then calcined in a muffle furnace at 500–550 °C for 3–4 hours to obtain zinc oxide nanoparticles. It is named as ZnO. The synthesized ZnO nano powder was collected, stored in airtight containers, and used for further characterization and application studies. Similarly for other metal Oxide too.

d. Synthesis of Zn-BiO Nanocomposite

Bismuth-doped ZnO nanoparticles were synthesized by adding few grams of zinc sulphate and few grams of sodium bismuth to 100 mL of aqueous *Hydrocotyle verticillata* leaf extract under continuous sonication at 35 °C for 4 hours. A color change from yellowish green to yellowish brown with increased turbidity indicated the formation of Zn–BiO precursor complexes mediated by phytochemicals. After the reaction, the mixture was cooled and filtered, and the filtrate was dried in a hot-air oven. The dried residue was then calcined at 500–550 °C for 3–4 hours in a muffle furnace to obtain Zn–BiO nanoparticles. The final nanopowder was collected and stored in airtight containers for further characterization and applications.

RESULTS AND DISCUSSION

a. UV -Visible analysis

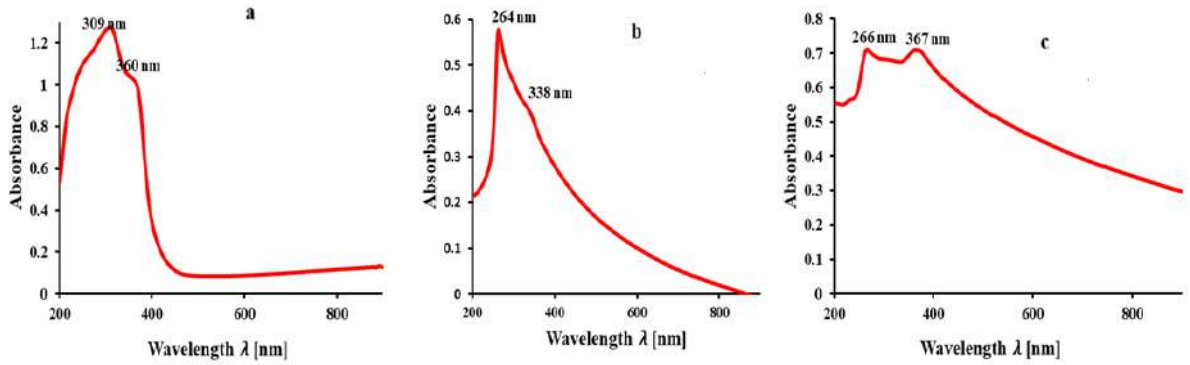

Figure1: UV-Vis spectrum of a) ZnO nanoparticles, b) BiO nanoparticles and c) Zn-BiO nanocomposite

ZnO nanoparticles show a UV absorption band at 309–360 nm due to band-gap transitions. The absorption edge (360 nm) is blue-shifted from bulk ZnO, indicating smaller particle size and quantum confinement, while no visible absorption confirms purity [1,2,5,6].BiO nanoparticles exhibit peaks at 264 nm and 338 nm, related to band-gap and charge-transfer transitions. The blue-shifted edge (338 nm) suggests reduced size and quantum confinement, with low visible absorption indicating good transparency and nanoscale formation [1,2,5,6]. Bi–ZnO nanocomposite displays peaks at 266 nm and 367 nm due to ZnO band-gap transitions and Bi-induced effects. The slight blue shift reflects reduced particle size, quantum confinement, and structural modification from Bi doping.

3.b. FT-IR Analysis

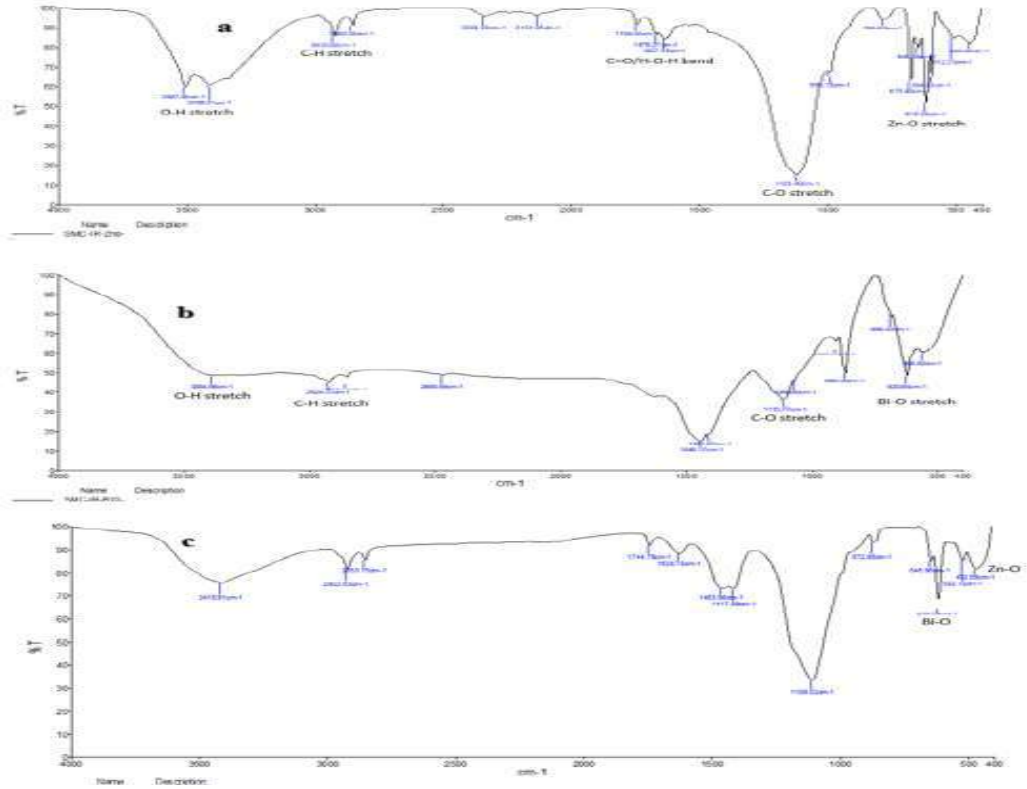

Figure 2: FT-IR Spectrum of a) ZnO nanoparticles b) BiO nanoparticles and c) Zn-BiO nanocomposite

ZnO nanoparticles shows broad bands at 3507 and 3409 cm^{-1} due to O–H stretching from surface hydroxyl groups and adsorbed water [3]. Peaks at 2923–2853 cm^{-1} correspond to C–H stretching from residual organics, while the band at 1745 cm^{-1} indicates C=O stretching. Signals around 1670–1637 cm^{-1} are attributed to H–O–H bending. These results confirm surface functional groups and successful ZnO formation [3,4]. BiO nanoparticles exhibit strong bands in the 500–600 cm^{-1} region, confirming Bi–O stretching and the formation of bismuth oxide [85,88]. The presence of hydroxyl and organic groups supports improved adsorption and photocatalytic activity. Zn–BiO nanocomposite shows a broad O–H band (3400–3600 cm^{-1}), C–H stretching (2920–2850 cm^{-1}), and H–O–H bending (1630–1650 cm^{-1}). Peaks at 1380–1400 cm^{-1} (N–O) indicate Bi incorporation, while 1050–1100 cm^{-1} (C–O) suggests organic–metal interactions [35]. Strong absorption at 450–600 cm^{-1} confirms Zn–O vibrations, with slight shifts indicating Bi–O–Zn bonding. Thus, FTIR confirms the successful formation of Bi–ZnO nanocomposite with modified optical properties.

c. X-RAY Diffraction Studies

The XRD pattern of the synthesized ZnO nanoparticles exhibits sharp peaks at 2θ values of 31.77°, 34.42°, 36.39°, 47.54°, 56.60°, 62.86°, and 67.96°, corresponding to the (100), (002), (101), (102), (110), (103), and (112) planes (JCPDS No. 36-1451) [27]. These peaks confirm the formation of highly crystalline hexagonal ZnO. The most intense peak at 36.39° ((101) plane) indicates preferential growth along this direction. The crystallite size (D) calculated using the Scherrer equation is found to be 26.88 nm, indicating that the particles are in the nanometer range. The XRD pattern of BiO nanoparticles shows sharp peaks at 2θ values of 28.43°, 32.86°, 47.15°, 52.91°, 56.05°, and 57.52°, corresponding to the (211), (222), (421), (430), (611), and (521) planes (JCPDS No. 96-153-7010) [28]. These peaks confirm a highly crystalline cubic BiO structure. The most intense peak at 32.86° ((222) plane) indicates preferential growth along this direction The crystallite size (D) calculated using the Scherrer equation is found to be 2.61 nm, indicating that the particles are in the nanometer range.The XRD pattern of the Zn–BiO nanocomposite shows diffraction peaks at 2θ values corresponding to the crystallographic planes (100), (101), (110), (111), (112), (200), (201), (210), (211), (220), (221), (310),

(311), (321), (322), (330), (331), (400), (411), (421), and (430), confirming the presence of both ZnO and BiO phases. The crystallite size (D) calculated using the Scherrer equation is found to be 1.94 nm, indicating that the particles are in the nanometer range. combined peaks of ZnO (JCPDS No. 96-230-0451, hexagonal) and BiO (cubic), confirming successful composite formation. Sharp peaks indicate good crystallinity, while slight shifts suggest lattice interaction and Bi in corporation [27,28].

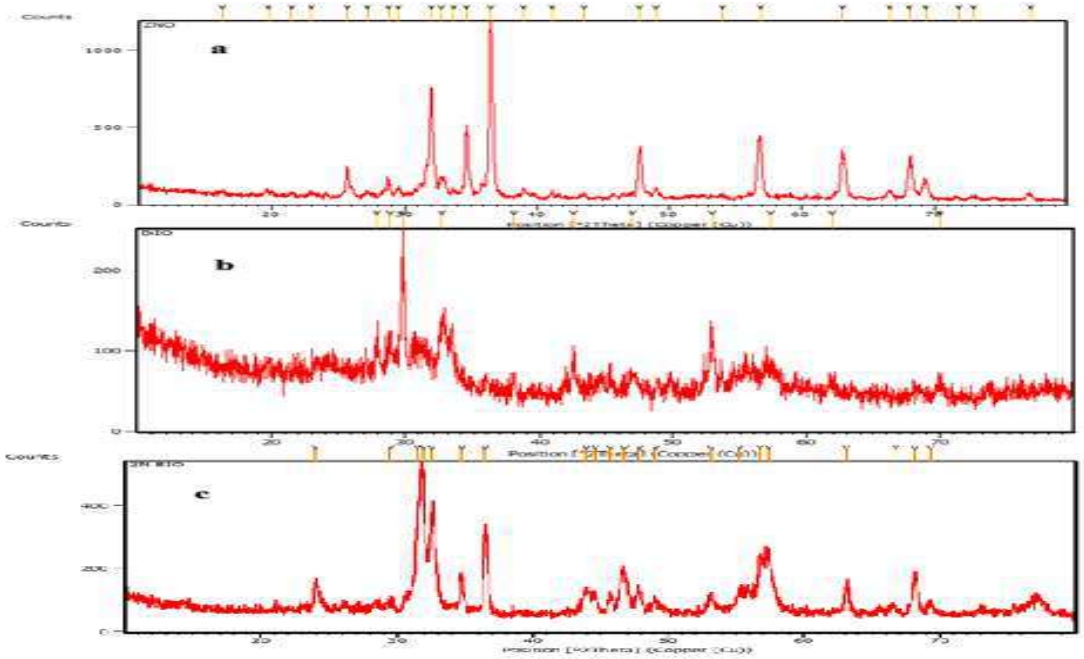

Figure 3: XRD spectrum of a) ZnO nanoparticles, b) BiO nanoparticles and c) Zn-BiO nanocomposite

d. Thermogravimetric Analysis (TGA)

The TGA curve of ZnO shows a total weight loss of 13.6% up to 1000 °C, with a high residual mass (86.4%), indicating excellent thermal stability. An initial 3.6% loss below 250 °C is due to moisture and volatile species removal. Gradual weight loss from 250–800 °C is attributed to decomposition of residual organics and hydroxyl groups, while a 7.9% loss above 800 °C corresponds to final organic removal and structural stabilization, confirming high purity [17-21]. BiO nanoparticles exhibit a total weight loss of 15.8% up to 1000 °C, with a high residual mass (84.2%) indicating good thermal stability. A 2.8% loss below 200 °C is due to adsorbed moisture removal. A 5.6% loss up to ~750 °C arises from decomposition of residual organics, followed by a 6.4% loss near 1000 °C due to lattice stabilization and removal of strongly bound impurities. The stable mass beyond this confirms the formation of crystalline, thermally stable BiO [17-21]. The nanocomposite shows a minor weight loss (1–2%) below 200 °C due to moisture and hydroxyl removal. A gradual decrease from 200–900 °C is linked to decomposition of residual precursors and crystallization of the mixed oxide system. A sharper loss near 950–1000 °C is associated with lattice rearrangement and interfacial interactions between ZnO and BiO, indicating good overall thermal stability [17-21].

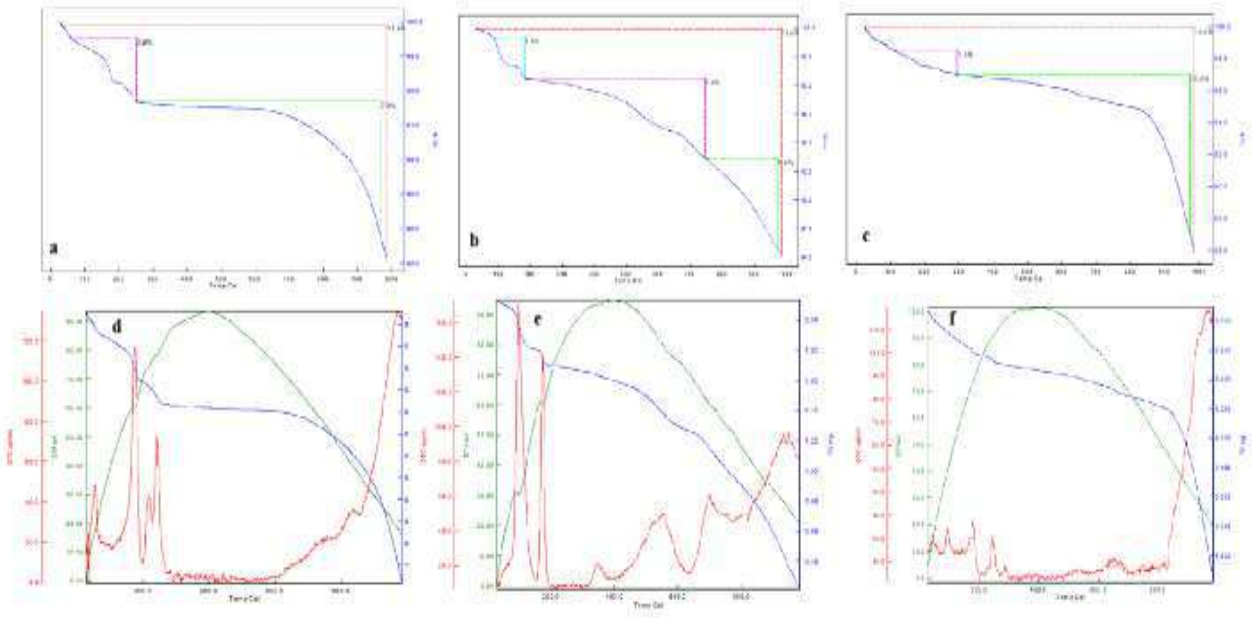

Figure 4: TGA of the synthesized a) ZnO nanoparticles, b) BiO nanoparticles c) Zn-BiO nanocomposite, d) curve of ZnO nanoparticles e) curve of BiO nanoparticles, and f) curve of Zn-BiO nanocomposite.

Thermogravimetric (TG), differential thermal analysis (DTA), and derivative thermogravimetric (DTG) analyses of the synthesized ZnO nanoparticles show that, 10–11% weight loss up to 1000 °C with high residual mass (80%), indicating good stability. Loss below 200 °C is due to moisture removal; 200–400 °C corresponds to organic decomposition and crystallization. Above 400 °C, minimal change confirms stable, phase-pure ZnO. Thermogravimetric (TG), differential thermal analysis (DTA), and derivative thermogravimetric (DTG) analyses of the synthesized BiO nanoparticles show initial loss below 200 °C due to moisture/precursors. Gradual loss (200–500 °C) from intermediate decomposition. Minimal change above 500 °C confirms formation of thermally stable crystalline BiO. Thermogravimetric (TG), differential thermal analysis (DTA), and derivative thermogravimetric (DTG) analyses of the synthesized Zn–BiO nanocomposite shows minor loss below 200 °C (moisture). Gradual loss from 200–500 °C due to precursor decomposition. Stable behavior above 500 °C indicates formation of thermally robust mixed oxide with strong ZnO–BiO interaction [17-21].

e. Field Emission Scanning Electron Microscopy (FESEM)

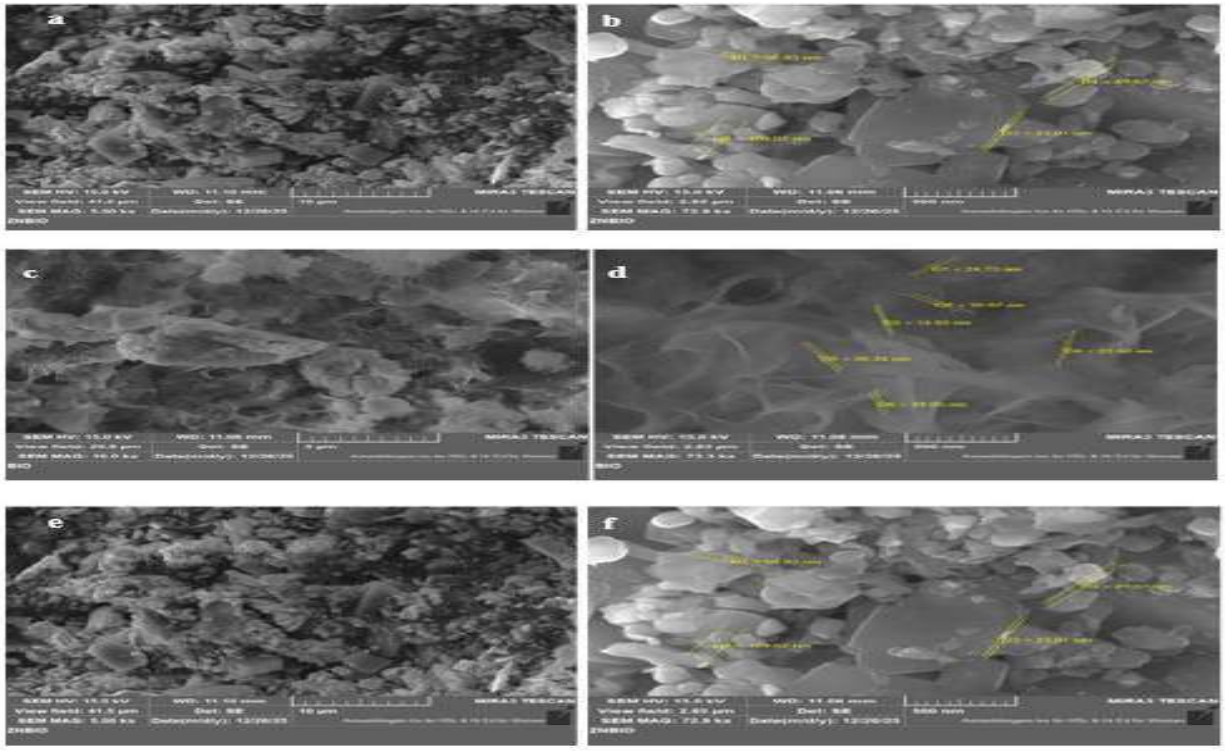

Figure 5: FESEM images of ZnO nanoparticles in different magnification a)50μm b)1 μm BiO nanoparticles in different magnification c)5 μm d)500nm, Zn-BiO nanocomposite with different magnification e)10 μm and f)500 nm.

The FESEM images of ZnO nanoparticles reveal well-defined rod-like and needle-shaped structures with relatively smooth surfaces. The particles appear randomly oriented and densely packed, forming clusters due to the high surface energy and strong interaction between nanoparticles. The FESEM images of the BiO sample reveal an irregular, flaky, and highly agglomerated morphology with rough and wrinkled surfaces. The particles appear as thin sheet-like or layered structures, randomly distributed and overlapping with each other. Such morphology is commonly observed in bio-derived materials where organic constituents influence the growth and aggregation of particles. The wrinkled and folded surface features indicate the formation of porous and loosely packed structures, which can significantly increase the effective surface area of the material. The FESEM images of the Zn–BiO composite reveals irregular and highly aggregated particles with a combination of plate-like, granular, and short rod-shaped structures distributed over the BiO matrix. The particles appear densely packed with uneven surfaces, indicating strong interaction between ZnO nanoparticles and the bio-organic matrix. The heterogeneous morphology suggests that the incorporation of ZnO into the BiO structure significantly alters the surface characteristics compared to the individual components.

f. EDAX ANALYSIS

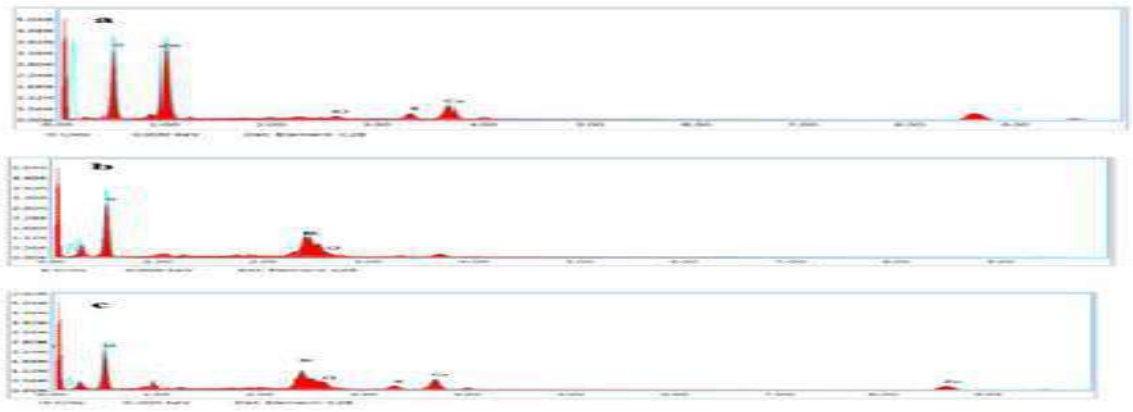

Figure 6: EDAX spectrum of a) ZnO nanoparticles b) BiO nanoparticles and c) Zn-BiO nanocomposite.

EDAX confirms Zn and O as major elements with strong Zn and O peaks. Weight %: Zn (58.71%), O (35.43%), with minor Cl and K traces from precursors. Absence of other impurities indicates high purity. EDAX shows Bi and O as dominant elements with strong characteristic peaks. Weight %: Bi (50.62%), O (45.91%), with minor Cl trace. Confirms pure bismuth oxide formation. EDAX confirms Zn, Bi, and O with strong peaks, indicating composite formation. Weight %: Zn (39.04%), O (27.84%), Bi (18.32%), with minor Ca and Cl traces. Results confirm good purity and successful synthesis.

Table 1: Elemental composition of ZnO, BiO nanoparticles and Zn-BiO nanocomposite

Sample	Element	Weight %	Atomic %
ZnO	Zn	58.71	27.51
	O	35.43	67.80
	Cl	1.38	1.18
	K	4.48	3.51
BiO	Bi	50.62	7.55
	O	45.91	89.41
	Cl	3.47	3.04
Zn-BiO	Zn	39.04	21.26
	Bi	18.32	3.12
	O	27.84	62.02
	Cl	3.67	3.69
	Ca	11.13	9.89

g. Antibacterial activity

Antibacterial activity of ZnO, BiO, and Zn–BiO was evaluated using the agar well diffusion method against *E. coli, S. aureus, B. subtilis, B. cereus,* and *K. pneumoniae*, with ciprofloxacin as control. Ciprofloxacin showed strong inhibition (22–34 mm), while nanoparticles exhibited moderate activity.

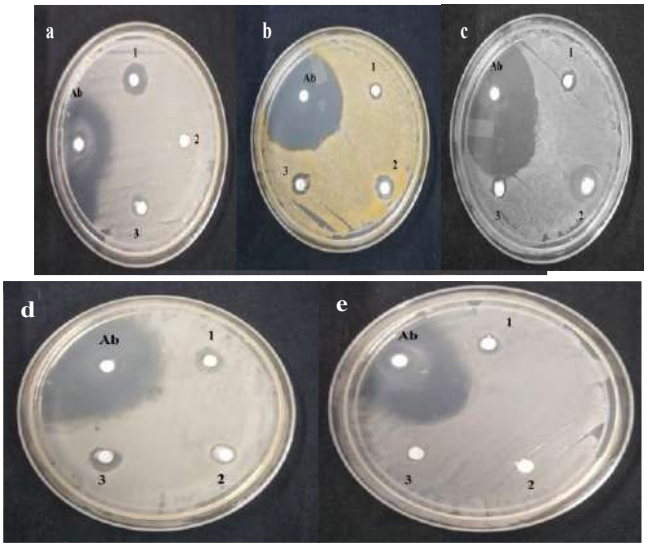

Figure 7: Antibacterial activity of ZnO, BiO and Zn-BiO nano in a) *E.coli* b) *Staphylococcus aureus* c) *Bacillus subtilis* d) *Bacillus cereus* e) *Kleibsiella pneumonia*

ZnO showed 5–10 mm inhibition, highest against *E. coli* (10 mm), due to ROS generation, Zn^{2+} release, and membrane damage [25]. BiO showed better activity against Gram-positive bacteria, especially *B. subtilis* (12 mm), but no effect on *E. coli* and *K. pneumoniae* [26]. The Zn–BiO composite showed moderate inhibition (6–7 mm) without significant synergy, likely due to agglomeration [24].

Table 2: Antibacterial activity of ZnO, BiO nanoparticles, Zn-BiO nanocomposite

Bacteria	Inhibition zone in mm			
	Ab ciprofloxacin	ZnO	BiO	Zn-BiO
E.coli	22	10	-	6
Staphylococcus aureus	32	5	7	7
Bacillus subtilis	34	6	12	6
Bacillus cereus	32	6	6	7
Kleibsiella pneumonia	27	5	-	-

Thus, Gram-positive bacteria were more susceptible than Gram-negative, and despite lower activity than ciprofloxacin, the nanoparticles demonstrate promising antibacterial potential.

h. Anticorrosion Activity

The anticorrosion performance of ZnO, BiO, and Zn–BiO coatings on mild steel was evaluated by the weight-loss method in acidic, basic, and neutral media over 9 days. Weight loss (ΔW) and inhibition efficiency were calculated by comparing coated and uncoated samples, with experiments conducted in triplicate.

All coatings reduced corrosion compared to the uncoated sample. ZnO showed effective protection, with lowest corrosion in neutral medium (0.51%), followed by acidic (1.14%) and basic (1.46%). BiO also exhibited good resistance, with best performance in neutral medium (0.42%), followed by acidic (0.91%) and basic (1.67%). The Zn–BiO composite showed improved performance, with maximum protection in acidic medium (0.85%), followed by neutral (0.58%) and basic (1.40%).

The uncoated sample showed higher corrosion rates in all media, especially in acidic and basic conditions. Thus, nanoparticle coatings significantly enhanced corrosion resistance, with neutral medium generally showing the best protection.

Table 3: Corrosion Rate (%) in Different Media

Medium	Sample	Wi (g)	Wf (g)	ΔW (g)	Corrosion Rate (%)
Acid	ZnO	7.6620	7.5840	0.0880	1.14
	BiO	7.8091	7.7375	0.0716	0.91
	Zn–BiO	7.6982	7.6320	0.0662	0.85
Base	ZnO	7.7511	7.6373	0.1138	1.46
	BiO	7.7685	7.6384	0.1301	1.67
	Zn–BiO	7.7278	7.6190	0.1088	1.40
Neutral	ZnO	7.7537	7.7141	0.0396	0.51
	BiO	7.7698	7.7366	0.0332	0.42
	Zn–BiO	7.7346	7.6890	0.0456	0.58

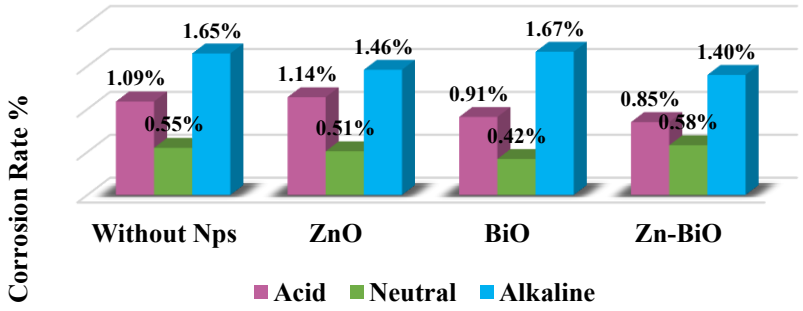

Figure 8: Corrosion Rate (%) of Samples in Different Media

Table 4: Anticorrosion Efficiency (%) of ZnO , BiO nanoparticles and Zn–BiO nanocomposite

Sample	Medium	Without NP (%)	With NP (%)	ΔW (%)	Anticorrosion Efficiency (%)
ZnO	Acidic	1.09	1.14	–0.05	–4.76
	Basic	1.65	1.46	0.19	11.5
	Neutral	0.55	0.51	0.04	7.2
BiO	Acidic	1.09	0.91	0.18	16.5
	Basic	1.65	1.67	–0.02	–1.2
	Neutral	0.55	0.42	0.13	23.6
Zn-BiO	Acidic	1.09	0.85	0.24	22
	Basic	1.65	1.40	0.25	15.1
	Neutral	0.55	0.58	–0.03	–5.4

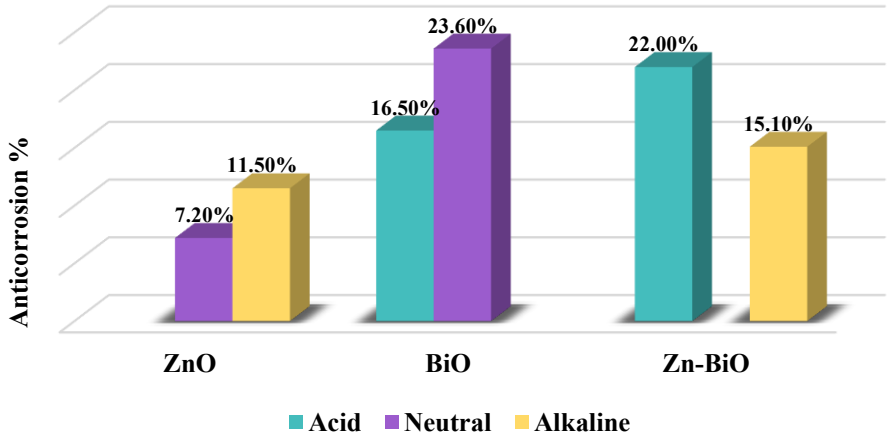

Figure 9: Anticorrosion Efficiency (%) of ZnO, BiO nanoparticles and Zn–BiO nanocomposite

CONCLUSION

Green synthesis offers a sustainable, eco-friendly, and cost-effective route for nanoparticle production using natural resources. In this work, *Hydrocotyle verticillata* leaf extract successfully facilitated the synthesis of ZnO, BiO, and Zn–BiO nanoparticles, where phytochemicals acted as natural reducing and stabilizing agents.

Optical studies indicated that ZnO mainly absorbs in the UV region, while BiO shows better visible-light absorption. The Zn–BiO nanocomposite exhibited a red shift and modified band gap, confirming enhanced visible-light responsiveness due to doping. FTIR analysis verified the formation of Zn–O and Bi–O bonds.

XRD results confirmed good crystallinity, with ZnO showing a hexagonal structure (26.88 nm), BiO a monoclinic phase (2.61 nm), and Zn–BiO a reduced crystallite size (1.94 nm), indicating successful Bi incorporation and suppressed crystal growth. This size reduction enhances surface area and potential catalytic activity.

TGA analysis demonstrated high thermal stability for all samples, with the Zn–BiO composite showing improved stability due to strong interfacial interactions. FESEM images revealed uniform ZnO particles, slight BiO aggregation, and better dispersion in Zn–BiO, while EDX confirmed elemental purity and successful doping.

Biological studies showed moderate antibacterial activity for ZnO and BiO, whereas the Zn–BiO composite did not exhibit significant synergistic improvement. In corrosion studies, ZnO performed well in basic media, BiO in neutral conditions, and Zn–BiO showed superior efficiency in acidic environments due to better surface protection.

Although ZnO and BiO have individual strengths, the Zn–BiO nanocomposite stands out as the most promising material due to its enhanced structural properties, improved corrosion resistance, and multifunctional applications.

REFERENCES

1. Alprol, A.E., et al. (2023). Algal Extracts for Green Synthesis of Zinc Oxide Nanoparticles: Promising Approach for Algae Bioremediation. Materials, 16, 2819. https://doi.org/10.3390/ma16072819
2. Mansour, A.T., et al. (2022). Green Synthesis of Zinc Oxide Nanoparticles Using Red Seaweed for the Elimination of Organic Toxic Dye from an Aqueous Solution. Materials, 15, 5169. https://doi.org/10.3390/ma15155169
3. Jeevanandam, J.; Chan, Y.S.; Danquah, M.K. Biosynthesis of metal and metal oxide nanoparticles. ChemBioEng Rev. 2016, 3, 55–67.
4. Miettinen, M.; Khan, S.A. Pharmaceutical pollution: A weakly regulated global environmental risk. Rev. Eur. Comp. Int. Environ. Law 2022, 31, 75–88.
5. Srivastava, V.; Gusain, D.; Sharma, Y.C. Synthesis, characterization and application of zinc oxide nanoparticles (n-ZnO). Ceram. Int. 2013, 39, 9803–9808.
6. Agarwal, H., Kumar, S. V., & Rajeshkumar, S. (2017). A review on green synthesis of zinc oxide nanoparticles – an eco-friendly approach. Resource-Efficient Technologies, 3(4), 406–413.
7. El-Saadony, M. T., et al. (2024). Green synthesis of metal oxide nanoparticles using plant extracts and their biological activities. Applied Nanoscience, 14, 225–238.
8. Vázquez-Muñoz, R., et al. (2020). Bismuth- and zinc-based nanoparticles: synthesis, characterization and multifunctional applications. Frontiers in Nanotechnology, 2(10).
9. Ahmed, K., & Li, J. (2021). Sodium bismuthate-based nanocatalysts: synthesis, properties, and photocatalytic activity. Journal of Environmental Chemical Engineering, 9(4), 105635.
10. Wang, J., et al. (2023). Enhanced visible-light photocatalysis of Ag-doped ZnO–$NaBiO_3$ nanocomposites synthesized by green route. Applied Catalysis B: Environmental, 328, 122426.
11. Murughu Gurusamy et al. (2024). Eco-friendly synthesis and enhanced antimicrobial activity of doped $NaBiO_3$/ZnO nanocomposites. Journal of Environmental Chemical Engineering, 12(5), 112345.
12. Sharaf, I. M., Koubisy, M. S. I., Alkallas, F. H., Trabelsi, A. B. G., & Aboraia, A. M. (2025). Tailoring β-Bi_2O_3 nanoparticles via Mg doping for superior photocatalytic activity and hydrogen evolution. Catalysts, 15(6), 519. https://doi.org/10.3390/catal15060519
13. Zav'yalova, A. A., & Imamov, R. M. (1972). Special features of the crystal structure of bismuth oxides. Zhurnal Strukturnoi Khimii, 13, 869–873.
14. Özgür, Ü., Alivov, Y. I., Liu, C., Teke, A., Reshchikov, M. A., Doğan, S., Avrutin, V., Cho, S.-J., & Morkoç, H. (2005). A comprehensive

review of ZnO materials and devices. Journal of Applied Physics, 98(4), 041301. https://doi.org/10.1063/1.1992666

15. Zhang, L., Wang, W., Yang, J., Chen, Z., Zhang, W., Zhou, L., & Liu, S. (2020). Sonochemical synthesis of Bi_2O_3 nanoparticles with enhanced photocatalytic performance. Ultrasonics Sonochemistry, 60, 104762. https://doi.org/10.1016/j.ultsonch.2019.104762
16. Zhou, Y., Liu, Y., & Zhang, H. (2021). Structural and microstrain analysis of metal oxide nanocomposites using Williamson–Hall approach. Ceramics International, 47(10), 13845–13853. https://doi.org/10.1016/j.ceramint.2021.01.234
17. Jebali, M., Colangelo, G., & Gómez-Merino, A. I. (2023). Green synthesis and TGA analysis of ZnO nanoparticles. Materials, 16(4), 1542. https://doi.org/10.3390/ma16041542
18. Ahmed, S. A., et al. (2024). Green synthesis and thermal analysis of ZnO nanoparticles. Discover Chemistry. https://doi.org/10.1007/s44371-024-00007-9
19. Khatami, M., et al. (2024). Thermal stability investigation of ZnO nanoparticles. RSC Advances. https://doi.org/10.1039/D4RA02452D
20. Kołodziejczak-Radzimska, A., & Jesionowski, T. (2014). Zinc oxide—From synthesis to application: A review. Materials, 7, 2833–2881. https://doi.org/10.3390/ma7042833
21. Umar, A., & Hahn, Y. B. (2010). Metal oxide nanostructures and their applications. Progress in Materials Science, 55, 653–726. https://doi.org/10.1016/j.pmatsci.2010.04.001
22. .Balci, M. (2024). Structural, thermal, surface, and electrical properties of Bi_2O_3 ceramics co-doped with Er–Ho–Tb rare earths. Journal of the Australian Ceramic Society, 60, 385–397. https://doi.org/10.1007/s41779-024-01007-9
23. Meher, A., Palai, A., Panda, N. R., Pati, S. P., & Sahu, D. (2025). Synthesis of zinc oxide/bismuth oxide nanocomposite photocatalyst for visible light-assisted degradation of synthetic dyes and antibacterial application. Environmental Science and Pollution
24. Reda, F. M., Hassan, A., & El-Sayed, M. (2024). Nanoparticle–bacteria interactions: Influence of cell wall structure on antibacterial activity of nanomaterials. Journal of Nanobiotechnology, 22, 1–15.
25. Alex, J., & Mathew, T. V. (2023). Surface modification of bismuth oxide nanoparticles with biotinylated β-cyclodextrin as a biocompatible therapeutic agent for anticancer and antimicrobial applications. Molecules, 28(8), 3604. https://doi.org/10.3390/molecules28083604
26. Bismuth oxide (α-Bi_2O_3). (2025). Antibacterial properties and applications of bismuth oxide nanoparticles. Materials Science Research Journal.
27. Schreyer Martin, Guo Liangfeng, Thirunahari Satyanarayana, Gao Feng, Garland Marc, "Simultaneous determination of several crystal structures from powdermixtures: the combination of powder X-ray diffraction, band-targetentropy minimization and Rietveld methods", Journal of Applied Crystallography 47(2), 659-667 (2014)
28. Zav?yalova A.A., Imamov R.M., "Special features of the crystal structure of bismuth oxides", Zhurnal Strukturnoi Khimii (Issue-No. from 1981) 13, 869-873 (1972).
29. Pal, G.; Rai, P.; Pandey, A. Green synthesis of nanoparticles: A greener approach for a cleaner future. In Green Synthesis, Characterization and Applications of Nanoparticles; Elsevier: Amsterdam, The Netherlands, 2019; pp. 1–26.

HOW TO CITE: J AshaJyothi, Carolin Jeniba Rachel, Savari Susila, Plant-Mediated Green Synthesis, Characterization and Applications of ZnO, BiO Nanoparticles and Their Zn-BiO Nanocomposite, Int. J. Sci. R. Tech., 2026, 3 (4), 528-539. https://doi.org/10.5281/zenodo.19607821